Published in final edited form as:
*Sens Actuators B Chem*. 2014 March 1; 192: 697–707. doi:10.1016/j.snb.2013.10.084.

# Polydimethylsiloxane Core-Polycaprolactone Shell Nanofibers as Biocompatible, Real-Time Oxygen Sensors

**Ruipeng Xue**[a], **Prajna Behera**[b], **Joshua Xu**[a], **Mariano S. Viapiano**[b], and **John J. Lannutti**[a,*]

[a]Department of Materials Science and Engineering, The Ohio State University, Columbus, OH 43210, USA

[b]Department of Neurosurgery, Brigham and Women's Hospital, Harvard Medical School, Boston, MA 02115, USA

## Abstract

Real-time, continuous monitoring of local oxygen contents at the cellular level is desirable both for the study of cancer cell biology and in tissue engineering. In this paper, we report the successful fabrication of polydimethylsiloxane (PDMS) nanofibers containing oxygen-sensitive probes by electrospinning and the applications of these fibers as optical oxygen sensors for both gaseous and dissolved oxygen. A protective 'shell' layer of polycaprolactone (PCL) not only maintains the fiber morphology of PDMS during the slow curing process but also provides more biocompatible surfaces. Once this strategy was perfected, tris(4,7-diphenyl-1,10-phenanthroline) ruthenium(II) (Ru(dpp)) and platinum octaethylporphyrin (PtOEP) were dissolved in the PDMS core and the resulting sensing performance established. These new core-shell sensors containing different sensitivity probes showed slight variations in oxygen response but all exhibited excellent Stern-Volmer linearity. Due in part to the porous nature of the fibers and the excellent oxygen permeability of PDMS, the new sensors show faster response (<0.5 s) −4–10 times faster than previous reports – than conventional 2D film-based oxygen sensors. Such core-shell fibers are readily integrated into standard cell culture plates or bioreactors. The photostability of these nanofiber-based sensors was also assessed. Culture of glioma cell lines (CNS1, U251) and glioma-derived primary cells (GBM34) revealed negligible differences in biological behavior suggesting that the presence of the porphyrin dyes within the core carries with it no strong cytotoxic effects. The unique combination of demonstrated biocompatibility due to the PCL 'shell' and the excellent oxygen transparency of the PDMS core makes this particular sensing platform promising for sensing in the context of biological environments.

### Keywords

nanofiber; co-axial; cytotoxicity; oxygen probes; bleaching

*Corresponding author. Phone: +1 614-292-3926. Fax: +1 614-688-3182. lannutti.1@osu.edu Address: 477 Watts Hall, 2041 College Rd., Columbus, OH 43210, USA.

## 1. Introduction

Oxygen is a vitally critical component of biological energy metabolism and plays a central role in many cellular processes.[1] In solid tumors, oxygen distributions are highly heterogeneous and are, in general, at much lower levels of oxygen than normal tissues.[2] The median $pO_2$ reading within breast cancer tumors was 30 mm Hg but is 65 mm Hg in normal breast tissue.[3] At these very low oxygen conditions cancer cells resist both radiotherapy and chemotherapeutics.[4, 5] Understanding how the biophysical properties of migration and sensitivity to chemotherapeutics are related to the surrounding oxygen content *in vitro* is key to the development of anti-migratory drugs. Thus, real-time continuous monitoring of local oxygen contents at the cellular level is desirable for the study of cancer cell biology. In addition, proper oxygen levels have significant effects on cell culture in tissue engineering.[6] Sensors that can determine dissolved oxygen in either standard culture or in a bioreactor can provide information critical to the design and operation of cell expansion processes.

Conventional Clark electrodes have dominated the oxygen sensor field thanks to their reliability and lack of heavy metal interference.[7] However, these sensors consume oxygen during measurements, are invasive and difficult to miniaturize to provide localized oxygen information. Recently, optical sensors based on luminescence quenching of oxygen sensitive probes (typically organometallic complexes and metalloporphyrins) have attracted a great deal of attention.[8] They are sensitive, inexpensive, non-invasive, more easily miniaturized and do not consume oxygen. In these sensors, the luminescence of the oxygen sensitive probes can be efficiently deactivated by the presence of molecular oxygen. The degree of this dynamic quenching is directly (linearly under ideal conditions) related to the environmental oxygen concentration and the corresponding intensity or lifetime is then used as indication of oxygen content.[9] This molecular probe is usually doped within protective polymer matrix materials (commonly in the forms of films) that serve as a solvent for the luminescent molecules, provide mechanical support, help improve selectivity by preventing penetration of interfering species and, most importantly, adjust the quenching behavior of the sensor by tailoring the probe-matrix interactions.[10] While these optical sensing films are disposable, sensitive and specific to oxygen, they are usually not very compatible with standard cell culture devices and in general have longer response times due to a 2D configuration that limits the surface area susceptible to rapid oxygen diffusion.

Biological applications require that these sensors function in an environment in which oxygen concentrations vary over a relatively small range. Therefore, high sensitivities are considered desirable. These high sensitivities could be accomplished by exploring both suitable polymer and/or oxygen probe combinations. A key component of an optical sensor is probe molecules that respond to oxygen by exhibiting changes in intensity and lifetime. The indicator should have good quantum yield and sufficient separation between the absorption and the emission peak (Stoke’s shift). This facilitates easy detection and measurement of any luminescence changes. The luminescence of the probe should be efficiently deactivated (quenched) in the presence of environmental oxygen. Generally, this requires that the excited electronic state of the dye be relatively long to increase the probability of collision between the probe and molecular oxygen.[11] Other desired

properties include photostability, inexpensive excitation and compatibility with supportive materials. The frequently used probe, tris(4,7-diphenyl-1,10-phenanthroline) Ru(II) (Ru(dpp)) is reported to have a long lifetime of 6.4 μs making it quite sensitive to molecular oxygen.[12] It has high quantum yield and is chemically, thermally and photochemically stable.[13] The relatively low saturation intensity enables the use of common low cost light sources such as light emitting diodes (LED) to provide sufficient excitation. Another good candidate probe, platinum octaethylporphyrin (PtOEP), shows high yield phosphorescence at 645 nm and possesses an excited triplet state lifetime as long as 75 μs.[14] That gives the probe very high oxygen sensitivity. The luminescence has larger Stokes shift compared with ruthenium based probe and displays excellent photostability.[15] These make it ideal for oxygen sensing especially under conditions of lower oxygen concentration.

In terms of matrix materials, the ideal polymer host should have high oxygen permeability, good mechanical support, stable chemical properties and good solubility for the probe molecules to prevent agglomeration. The major forms are polymer films produced by techniques such as spin coating or dip coating in which physically incorporated or covalently bonded oxygen probes are contained within the matrix. Highly gas permeable polymers provide easy access to oxygen entering the matrix and homogeneously distributed probes can then give sensitive, linear responses to the infusing oxygen molecules. Various matrix materials have been used as hosts including silicone rubbers, polystyrene, poly(vinylchloride), hydrogels and sol-gels.[16–20] Among these candidate host materials, polydimethylsiloxane (PDMS) films have been extensively studied due to their extremely high $O_2$ permeability, transparency and chemical stability. However, nonlinear calibration curves are often observed for silicone-based sensors.[21] The need for cross-linking also limits the application of PDMS to complex 3D scaffolds for biological applications. In addition, PDMS is highly hydrophobic and such surfaces typically make poor substrates for mammalian cells.[22]

In spite of these barriers, the extraordinary gas permeability of PDMS is very attractive. To take advantage of this property while improving the response time of the 2D film-type optical oxygen sensors, we fabricate nano-scaled PDMS fibers containing oxygen-sensitive probe molecules covered by a protective polycaprolactone (PCL) ‘shell’ layer by electrospinning and explore the sensing performance of the resulting fibers. Such electrospun fibers potentially have wide applications in cancer research and tissue engineering. However, the need to cross-link PDMS monomers remains a key stumbling block that limits our ability to electrospin PDMS since as-spun, uncrosslinked nanofibers are in the liquid state and form films following deposition. We chose to make PDMS-PCL core-shell structured fibers that immobilize the oxygen probes inside the PDMS core while still allowing utilization of PDMS’ high gas permeability. Outside the core, a thin PCL shell helps maintain the fiber morphology prior to and during cross-linking while adding excellent biocompatibility for cell attachment and migration. To fully explore the advantages provided by this new concept, three oxygen-sensitive probes and two different PDMS matrices are fabricated to establish the effects on properties associated with oxygen sensing in biological systems. The three sensing probes are from two most representative categories (ruthenium-based complexes and platinum-based porphyrin) that include different counterions to explore the effects of probe solubility. In addition, we cultured CNS1, U251 and GBM34

cell lines on these as-spun core shell fibers to determine whether the presence of the porphyrin dyes within the core carried with it significant cytotoxic effects. The resulting electrospun fiber platform appears to be both biocompatible and has the capability to report local oxygen contents to provide valuable information establishing the relationship between cell migration and locally variable hypoxic conditions.

## 2. Experimental

### 2.1. Materials

Polycaprolactone (Mn=70,000–90,000) was purchased from Sigma-Aldrich (St. Louis, MO, USA). Silastic® T-2 two-part silicone was obtained from Dow Corning Corporation (Midland, MI, USA) and Permatex® one-part moisture cure room-temperature vulcanizing (RTV) silicone was purchased from Illinois Tool Works Inc. (Hartford, CT, USA). Oxygen sensing probes, tris(4,7-diphenyl-1,10-phenanthroline) ruthenium(II) dichloride (Ru(dpp)(Cl)), tris(4,7-diphenyl-1,10-phenanthroline) ruthenium(II) tetraphenylboron (Ru(dpp)(PB)) and platinum (II) octaethylporphine (PtOEP) were acquired from Alfa Aesar (Ward Hill, MA, USA). 1,1,1,3,3,3-hexafluoro-2-propanol (HFP) was obtained from Oakwood Products Inc. (West Columbia, SC, USA). Dichloromethane (DCM) and toluene were also obtained from Sigma-Aldrich.

### 2.2. Instruments

Scanning electron microscopy (SEM) (FEI Company, Hillsboro, OR, USA) was used to examine the morphology of the electrospun core-shell following the application of a thin gold coating. Luminescence images of the fibers were captured on a fluorescence microscope (Nikon Inc. Melville, NY, USA) using a filter set for red fluorescence (EX: 530–560 nm, DM: 570 nm, BA: 590–650 nm). The luminescence spectra of the core-shell fibers and the strip chart for the emission peak as function of time were recording using a fluorescence spectrometer (Ocean Optics Inc., Dunedin, FL, USA). Blue LED light at 470 nm was guided through the 600 μm VIS-NIR fibers to act as the excitation source. The optic probe of the spectrometer was fixed to directly point at the experimental samples.

### 2.3. Fabrication of electrospun core-shell fibers

The PCL solution used for the shell of electrospun fibers was fabricated by dissolving 5 wt% PCL in HFP to form a uniform, clear solution. Solutions intended for the oxygen-sensitive core of the fibers were made by dissolving the luminescence probes in appropriate solvents containing the corresponding silicones. Typical weight ratios of probe to silicone for Ru(dpp)(Cl) in T-2 PDMS were 1:1000 and the two part silicone solution (base: curing agent=10:1 by weight) concentration in DCM/toluene mixture (3:2 by weight) was 20 wt%. For the RTV silicone solution, 5 mg Ru(dpp)(B) was dissolved in 20% RTV silicone solution containing 1 g silicone. The same 1:200 dye-polymer weight ratio and polymer concentration were applied for PtOEP/RTV silicone system with chloroform as the solvent for PtOEP and PDMS. Core-shell fibers were produced by a simultaneous co-axial electrospinning of two polymer solutions through two concentric blunt needles. In all cases a flow of 1 mL/h was used for the ‘core’ and 4 mL/h for the ‘shell’ solution. A high voltage DC power supply (Glassman High Voltage, Inc., High Bridge, NJ, USA) set to be 25 kV and

a 20 cm tip-to-substrate distance was used for all electrospinning processes. As-spun Silastic® 'core' fibers were held at room temperature for 24h before use to allow the core to fully cure. For the Permatex® moisture cure silicone, the samples were placed in a sealed container maintained at a relative humidity >80%.

### 2.4. Gaseous oxygen sensing performance

The sensing fiber mats were cut into 1 × 1 cm squares and glued on edge to the inner wall of a glass bottle. The oxygen gas concentration was controlled by adjusting the relative flow rates of oxygen and nitrogen by a gas mixer (Omega Engineering, USA). Spectra were recorded by the SpectraSuite software of the spectrometer when the environmental oxygen reached equilibrium. The reversibility and response time were revealed from the intensity change of the emission peak as the environment was cycled between pure nitrogen and oxygen.

### 2.5. Dissolved oxygen sensing performance

A similar arrangement involving a large glass container was used to immerse the sample into water to measure the intensity changes in response to variations in dissolved oxygen. The glass bottle was contained within a water bath so that temperature could be precisely controlled. The desired gas mixtures emerging from the gas proportioner were used to sparge the water for a sufficiently long (~30 minutes) time to ensure that equilibrium was reached prior to measurement. A commercial oxygen meter (Hach Company, Loveland, Colorado, USA) was used to correlate the intensity of the core-shell fiber with the real oxygen content measured by the meter. The reversibility and photobleaching data in solution were obtained by continuously monitoring the emission peak versus the dissolved oxygen level and time.

### 2.6. Cell culture experiments

To establish whether these oxygen-sensing fibers were cytotoxic to cells representative of the intended application, cell culture experiments were performed with two well-established glioblastoma cell lines (U251MG and CNS1) as well as a primary culture of glioblastom stem-like cells (GBM34). U251MG cells were cultured in Dulbecco's modified Eagle's medium (DMEM, containing 4.5 g/L glucose and 10% v/v fetal bovine serum) while CNS1 cells were cultured in RPMI-1640 medium (containing 2 mM L-glutamine and 10% v/v fetal bovine serum. GBM34 cells were cultured in DMEM containing F-12 nutrient mixture (DMEM/F12), supplemented with 2mM L-glutamine, 20 ng/ml human epidermal growth factor, 20 ng/ml human basic fibroblast growth factor, 2 μg/ml porcine heparin, and the vitamin supplement B27 (Invitrogen). All media included). 50 UI/ml penicillin and 50 μg/ml streptomycin to prevent bacterial growth.

To assess viability, 15 mm round glass coverslips were coated with PCL or PDMS(PtOEP)-PCL nanofibers and placed in 24-well plates. Wells were washed with phosphate buffered saline and coated with bovine fibronectin (5 μg/ml, Invitrogen) for 2 hours at room temperature, as described.[23] Cells were gently dissociated when they reached 80% confluence and seeded at an average density of 10,000 cells/well. Cells were cultured for 48 hours and subsequently co-stained with Calcein-AM (1 μg/mL, Invitrogen) and propidium

iodide (0.5 μg/mL, Invitrogen), following standard protocols. Fluorescence microscopy was used to quantify live (calcein-positive, green fluorescence) and dead (PI-positive, red fluorescence) cells. Image analysis and automated cell counting were performed using ImageJ (v.1.47) software.

To quantify cell migration on nanofibers, cells were trypsinized and cultured at low density in ultralow-attachment 96-well plates (Corning) for 48 hours, in order to form suspended tumorspheres (350–400 m diameter). Tumorspheres were individually seeded on nanofiber coated-slides and imaged by fluorescence microscopy to analyze cell migration. The dispersion of the cells after 48 hours was measured as described [23] and used to calculate the cell migration index ($t_{48}/t_0$).

## 3. Results and discussion

### 3.1. Results of PDMS-PCL core-shell fiber oxygen sensing performance

**3.1.1. Compositions of PDMS-PCL fibers containing oxygen sensitive probe—** Three combinations of sensing probe and PDMS fibers were fabricated and the specifications are listed in Table 1. We observed that the addition of the oxygen probe to the PDMS matrices slowed down or even interrupted the curing process of the two-part PDMS. Thus, for sample S1, only 0.1% of Ru(dpp)(Cl) could be loaded into the two-part PDMS core of the fibers without delaying curing. On the other hand, moisture cure PDMS was observed to be much less sensitive to the presence of the probe molecules. For sample S2, Ru(dpp)(PB) was embedded in the moisture cured PDMS to increase probe solubility in PDMS due to its hydrophobic property allowing up to a 0.5% weight doping ratio. The same probe 0.5% concentration was successfully used for moisture cured PDMS fibers containing PtOEP (S3).

**3.1.2. Morphology of the core-shell fibers—**The morphology and luminescence of electrospun PDMS core, PCL shell fibers containing Ru(dpp)(Cl) in the core (S1) is shown in Figs. 1A and 1B. The relative flow rate of the core and shell polymer solutions during electrospinning is a critical factor controlling the formation of PDMS-PCL fibers and final sensing properties of the core-shell fibers. The PDMS core as-spun is in its viscous state and would normally produce a film under these deposition conditions. The high PCL shell flow rate helps ensure the ‘electrospinnability’ of these core-shell fibers. However, a too-thick PCL shell would increase the diffusion path length of oxygen in the PCL shell that has lower permeability than the PDMS core. In this paper, the relative core and shell flow rates were fixed at a ratio of 1:4. Similar fibers could also be achieved for S2 and S3 samples as shown in the SEM (Figs. 1C and 1E) and fluorescent images (Figs. 1D and 1F). Higher probe solubility makes individual fibers of S2 brighter than S1. Comparable fluorescent images could be obtained for both samples but with different acquisition times (600 ms for S1 and 200 ms for S2). There is no significant morphological difference for these PDMS-PCL core-shell fibers compared to alone PCL fibers (images not shown). The fiber diameters (average ± standard deviation) of all three samples are also listed in Table 1.

**3.1.3. Sensitivity to gaseous phase oxygen—**Gaseous oxygen concentration was gradually increased (in 10% intervals) and the corresponding spectra of emission plotted in

Fig. 2. The Ru(dpp)(Cl) in S1 core-shell fibers absorb visible light at 455 nm and emit red luminescence at 618 nm. The intensity of the emission peak of core-shell fibers was efficiently quenched as the oxygen concentration increased gradually from 0 to 100% as in Fig. 2A. No peak shift was observed when increased levels of oxygen were introduced into the environment. The saturated peak on the left originates from the blue LED light excitation. A similar spectral response is observed in Fig. 2C for sample S2 along with a higher degree of quenching and a red shift to 622 nm. Due to the higher probe concentration, the emission peaks of sample S2 exhibited less overlap with the light source peak. The same test of sample S3 generated significantly different spectral shapes and responses to gaseous oxygen (Fig. 2E). The emission peak for S3 is at 645 nm and is sharper compared to samples with Ru probe.

The dynamic quenching process could be described by the Stern-Volmer equation [16]:

$$I_0/I=1+K_{SV}[O_2] \quad (1)$$

$$K_{SV}=k_2\tau_0 \quad (2)$$

$$\tau_0=1/k_1 \quad (3)$$

Where $I_0$ and I are luminescent intensity without and with the quencher, $[O_2]$ is the oxygen (quencher) concentration, $k_2$ is the bimolecular rate constant of the quenching process, $\tau_0$ is the lifetime of the excited state decay without quencher and $k_1$ is the rate constant for the decay. Figs. 2B, 2D and 2F show the Stern-Volmer data of PDMS-PCL fibers S1, S2 and S3 by monitoring the intensity of emission peaks at various oxygen concentrations. Also included are their linear fits. A simple representation of the sensitivity of the sensors could be the intensity ratio of the sensors when exposed to an oxygen-free environment or pure oxygen $I_0/I_{100}$. For sample S1, the $I_0/I_{100}$ value is 2.97 and the coefficient ($R^2$) for the linear fitting is 0.9932. Both sensitivity and linear fitting are improved for S2 with $I_0/I_{100}$ of 4.10 and $R^2$ of 0.9982. For PtOEP probe containing S3 sample, a six-fold higher $I_0/I_{100}$ value of 24 is obtained, a significant improvement in sensitivity. The linear calibration fitting is also very good ($R^2$=0.9983).

**3.1.4. Reversibility, response time and recovery time to gaseous phase oxygen—**When the sample was continuously monitored in rapidly alternated gaseous atmospheres, the intensity dropped and fully recovered when the environment was switched between pure nitrogen to oxygen as shown in Fig. 3. All three samples show good intensity reversibility and prompt response. S1 PDMS-PCL core-shell fibers showed 0.36±0.05 s response time and 0.72±0.27 s recovery time. Similar fast response and recovery were also observed for the two other samples. The response time was 0.28±0.08 s for S2 and its recovery time was 0.51±0.15 s. For sample S3, response and recovery time were 0.49±0.13 s and 0.70±0.15 s, respectively.

**3.1.5. Sensing performance - dissolved oxygen—**Fig. 4 shows the Stern-Volmer response of the core-shell fibers to dissolved oxygen. The oxygen concentration

(independently measured in parallel using the commercial meter) was carefully varied over a biologically-relevant range. The nanofiber sensors revealed excellent response to even very small variations in dissolved oxygen. Stern-Volmer constants ($K_{SV}$) calculated from Eq. (1) for S1, S2 and S3 are 0.04, 0.08 and 0.41 $(mg/L)^{-1}$, respectively. Similar to the trends for gaseous oxygen, S3 showed significantly higher sensitivity than S1 and S2. The fitting coefficients are equivalently high for all three fibers: $R^2$(S1)=0.9987, $R^2$(S2)=0.9990 and $R^2$(S3)=0.9992. Intensity was then continuously monitored when alternating oxygen and nitrogen were rapidly introduced to the solution as shown in the inserts of Fig. 4. The fibers showed reversible luminescence change in water but the response and recovery time were longer than the gas phase tests. The delay was apparently caused by the time required to saturate the solution with the appropriate gas. This is proven by the fact that the pattern of response/recovery could be altered significantly if the gas flow rate was varied.

**3.1.6. Stability—**The PDMS-PCL fibers were placed in water and were continuously illuminated by the blue LED light to record the signal change as function of time. To examine the effects of oxygen to photobleaching, tests were conducted in both oxygen-free and air-saturated water (Fig. 5, 'No $O_2$' vs. 'Air') for 1450 s (~24 minutes). For easy representation and comparison, data of all samples are shown in the same plot and the initial relative intensities are set to 1, 0.7 and 0.4 for S1, S2 and S3, respectively. As shown in Fig. 5, only sample S1 shows some noticeable intensity decay under continuous excitation. S1 in air-saturated water exhibited a faster rate of decrease (0.28% per minute) than the same sample measured in oxygen-free water (0.06% per minute). Less than 1% total intensity decay could be measured for S2 in both conditions after completion of the experiment. For sample S3, virtually no intensity decrease was detected following the light exposure.

**3.1.7. Oxygen-sensing nanofiber cytotoxicity—**To investigate cytotoxicity potentially caused by the presence of the Pt porphyrin within the PDMS core of these nanofiber sensors, both electrospun PCL without any probe molecules and the Pt probe-containing PDMS(PtOEP)-PCL nanofiber sensors(S3) were investigated using adherent cultures of different glioblastoma cell types, including highly-sensitive primary cultures of glioblastoma stem-like cells. Cell morphology on aligned versions of the different fiber compositions was essentially identical and there were no evident differences in cell stretching over the fibers (Fig. 6A). Cell dispersion was also undistinguishable between PCL and PDMS(PtOEP)-PCL fibers, indicating that cell adhesion and motility had not been affected by the Pt compound (Fig. 6B). Quantitative analysis of cell viability (Fig. 7A–B) and cell migration indicated that number of adhered cells per $mm^2$, proportion of viable cells, and cell migration index, were largely identical between PtOEP-containing nanofibers and PCL nanofibers, with minor differences that did not follow a common trend for the different cells analyzed. Overall, the presence of the platinum porphyrin within the PDMS core did not lead to consistent, significant cytotoxicity.

### 3.2. Discussion of PDMS-PCL fiber sensing performance

**3.2.1. Electrospinning of PDMS-PCL fibers—**Normally, fabricating PDMS fibers by electrospinning is challenging due to the resins' inherently slow curing process. Few reports of PDMS electrospinning exist and all involve relatively complex procedures.[24] In our

case, however, PDMS can be electrospun to form the unique core-shell structure in a single step due to the advantages conferred by containment within the PCL shell. When the falling fibers successfully reach the grounded collector, the PCL shell covering the uncured PDMS plays a critical role as it efficiently confines the relatively mobile liquid containing the uncured PDMS solution and prevents film formation. The cross-linking reactions (catalyzed either by the curing agent or by water) follow and morphologically stable PDMS-PCL core-shell fibers based optical oxygen sensors are created. Based on the SEM images, PDMS-PCL fibers show typical electrospun fiber morphology and dye loading has little influence on the structure of the core-shell fiber. Fiber diameters are generally in the range of 400–600 nm. The order of fiber diameter for the three samples is S2<S1<S3. Electrospun fiber diameter and morphology are dependent on various parameters such as polymer identity, solvent, solution concentration, applied voltage and flow rate.[25]

The cross-linking reaction for the two-part PDMS is initiated by the catalyst and occurs between PDMS base and curing agent. Although there is virtually no shrinkage during the reaction due to a lack of byproducts, the reaction rate is apparently decreased when the ruthenium complex is present. The evidence for this is the fact that attempts to use the same PDMS solution for S1 with high probe concentration to generate solid films instead maintained their liquid state for several days after addition of the curing agent, an observation we attribute to an unfavorable chemical interaction between the dye and the curing agent. Therefore, only 0.1wt% dye could be incorporated into S1 samples without loss of fiber morphology due to this interference with the curing process.

On the other hand, the curing of one-part moisture cure PDMS for S2 and S3 requires only the participation of ambient moisture and is virtually insensitive to the presence of the oxygen probe molecules. The porous nature of the fibers combined with the very high surface area assists in the curing process catalyzed by the ready availability of ambient moisture.

While improved curing allows for increased probe concentrations, another important factor concerns the solubility of the probe in the matrix. Ru(dpp)(Cl) is a chloride salt and is hydrophilic in nature and therefore solubility is limited in the hydrophobic PDMS matrix. Other work has shown that the hydrophilicity of the salt is mostly determined by the counterion and thus the Ru(dpp) complex can become lipophilic if the chloride is replaced by a hydrophobic counterion such as tetraphenylborate (PB).[26] In addition, the luminescence properties of the Ru complex with the hydrophobic counterion are virtually the same as its chloride salt-based counterpart and the sensing ability should not be influenced by modification of the ion pair.[27] As a result, the high Ru(dpp)(PB) probe doping in S2 does not cause any noticeable agglomeration while increasing the emission signal of the fibers. Similarly, high PtOEP could also be embedded in S3 without causing any problem either for curing or for probe dispersion.

**3.2.2. Luminescence of PDMS-PCL fibers—**The luminescence of the Ru based complexes used in S1 and S2 involves promotion of an electron from the metal d orbitals to a ligand antibonding orbital, a process known as metal-to-ligand charge transfer (MLCT).[28] After excitation, a triplet state could be reached from an excited singlet state by

intersystem crossing having a rate coefficient close to unity. Thus, fluorescence from the excited singlet to the ground state is rarely observed and emissions are mainly phosphorescent and have relatively long lifetimes. Quenching of the phosphorescence via dynamic collision with oxygen molecules is then used to report environmental oxygen concentrations. As shown in Fig. 2, the emission peaks of S1 and S2 have a similar shape due to the incorporation of the same Ru complex cation responsible for the luminescence. The hydrophobic counterion tetraphenylboron allows for higher dye concentrations in PDMS for S2 and also shifts the emission peak to 622 nm compared to low probe concentration S1 sample's 618 nm peak. The oxygen sensitive probe PtOEP used in S3 has a lifetime of 75 μs (versus 6.4 μs for the Ru probe), larger Stokes shift and greater photostability. The absorption in the visible range originates from the π to π* transition and the intersystem crossing to the triplet state enabling long-lived phosphorescence emission.[15] The emission peak (645 nm) is well separated from the excitation wavelength (535 nm). This efficiently eliminates the influence of the excitation source. The hydrophobic nature of PtOEP also allows its higher loading within the PDMS matrix at the same concentrations as in the S2 sample.

**3.2.3. Sensitivity to gaseous oxygen—**Since the triplet to ground state transition (emission of phosphorescence) is spin forbidden, the lifetime of phosphorescence is relatively long and is therefore susceptible to environmental deactivation (such as quenching) due to molecular oxygen.[29] Sensitivity can be directly observed from the spectral response when the samples are exposed to environments gradually varying from 0 to 100% oxygen. Due to the improved chemical accommodation of hydrophobic Ru(dpp)(PB), sample S2 shows higher $I_0/I_{100}$ (4.10) compared to 2.97 $I_0/I_{100}$ value obtained from S1 sample containing the hydrophilic chloride salt of the same complex. PtOEP has even longer lifetimes and therefore generally better sensitivity and much lower detection limits. The observed $I_0/I_{100}$ of 24 for sample S3 constitutes a dramatic improvement relative to Ru based oxygen detection in the same core-shell fibers. The sensing performance of oxygen sensors depends on probe properties, matrix identity, probe-matrix interactions and the overall sensor form. The sensitivity of other non-fibrous sensor systems spans a large range in which $I_0/I_{100}$ values vary from 1.1 to several hundred.[8, 9] The fibers incorporating Ru probes in the current study show sensitivity comparable to the physically embedded form of the same probe in either mesoporous silica or polystyrene film.[30, 31] On the other hand, the sensitivity ($I_0/I_{100}$ value) of PtOEP in the nanofibers appears to be higher than that observed when the same probe is dispersed in polystyrene (4) and polyethylmethacrylate films (16) but is lower than that observed in sol–gel (47) produced carriers.[32–34]

A major advantage of nanofibers over widely used films is that all three PDMS-PCL fibers exhibited excellent linearity over the entire range of oxygen concentrations (0–100%). In contrast, a downward Stern-Volmer curvature is observed in a variety of literature-based systems especially those based on silicone.[21, 26, 27, 35, 36] Accordingly, to produce a linear calibration curve, a multi-site Stern-Volmer model is often used.[37] In such cases, the probe is believed to present both its molecularly uniform state and an aggregated form each having distinct quenching constants. The ratio of these two forms will vary depending on the compatibility between the host polymer and the sensing probe. The slightly lower

fitting coefficient of S1 compared to S2 is attributed to the lower solubility of the hydrophilic version of the Ru complex in PDMS. An excellent linearity for Pt dye in the PDMS system indicates an excellent compatibility as observed by other studies.[38] A single quenching constant $K_{sv}$ can only be obtained when the sensing probe molecules are evenly dispersed in the matrix materials and have the equivalent opportunity for oxygen access. The excellent linear behavior of our PDMS-PCL fibers occurs because the speed of the electrospinning and evaporation process probably locks the solvated probe distribution in place.[39] The curing reaction rate for moisture cure PDMS is also accelerated due to the small fiber dimensions that provide constant, easy moisture access. This increased curing rate is important because in other studies that involve a longer curing time necessary for film formation (especially at elevated temperatures), probe molecules have been observed to migrate and aggregate to form regions having lower/different sensitivities.[36]

**3.2.4. Reversibility, response time and recovery time in gas phase oxygen—** PDMS-PCL core-shell fibers show short response times (less than 0.5 s) owing to the high surface-area-to-volume ratio that significantly reduces the barrier for oxygen diffusion to the molecular probe. In contrast, typical response times of film-based sensors varies from less than 1 second to tens of seconds depending upon the matrix.[8] Gas exchange for sensing films is limited to the 2D external surface and increasing film thickness (to enhance signal strength) increases diffusion depth and worsens the response time. However, the response time of PDMS-PCL core-shell fibers fibers does not change as mat thickness increases due to the inherently high porosity of electrospun fibers. Rapid response and recovery also attests to the exceptional oxygen permeability of PDMS and its suitability for inclusion as the core. This is additionally demonstrated by comparison to similar fiber-based systems that utilized Cu- or Eu-based fluorophores but display 4–10 times longer response times.[40–42] The room temperature oxygen diffusivity in PDMS is $4.1\times10^{5}$ $cm^2/s$, almost twice the diffusivity of oxygen in water ($2.1\times10^{5}$ $cm^2/s$) under the same conditions.[43] When used as sensor matrix in water, PDMS therefore provides relatively little barrier to oxygen diffusion to the probe and allows real-time reporting of oxygen levels. The recovery time is longer than the response time likely due to the fact that $N_2$ gas permeability and diffusivity in polymers is less than that of $O_2$. The response time of the PDMS-PCL sensors may also be related to the fiber diameter due to the observation that the order of response times for the three samples is the same as that of the fiber diameter (S2<S1<S3).

**3.2.5. Sensor performance to dissolved oxygen—**The dissolved oxygen concentration range explored (Fig. 4) covers a variety of circumstances that cells may encounter *in vivo*. Although 21% oxygen enters the lungs, dissolved oxygen in the body averages only 3–5%, depending on the tissue.[35] The fibers show high quenching constant $K_{SV}$ and excellent linear fit, which enables precise quantitative determination of oxygen concentration in the range of interest without the need for complex calibration equations. Due to the hydrophobic nature of PDMS, the embedded probe molecules are shielded from ionic species by the permeation selective nature of the surrounding matrix. Dissolved oxygen molecules must first escape from aqueous solution and penetrate the polymer matrix to reach the probe. The partial pressure of gaseous oxygen is in equilibrium with the dissolved oxygen and related by Henry's Law.[44] Therefore, the order of the three samples

in terms of sensitivity is the same as the gas phase tests (S3≫S2>S1) and the excellent Stern-Volmer data fittings still hold for all dissolved oxygen measurements.

The examination of real time PDMS-PCL response is critical for the sensor's future application so the same reversibility test was conducted in deionized water by again alternating nitrogen and oxygen exposure. While the environment itself took time to become saturated with $N_2/O_2$, the full sensor response only required about 10 s (Fig. 4). Considering the very fast response to gas phase oxygen (shown in Fig. 3), we can assume that ~95% of the time needed for the sensor to fully respond/recover is due mainly to the slowness of oxygen removal/dissolution and not the sensor itself.

**3.2.6. Stability—**Several observations could be summarized from the intensity decay curves in Fig. 5: a) photobleaching rate is obviously faster in the presence of oxygen for S1; b) S2 PDMS-PCL fibers show slower decay rate even though they have higher probe concentration than S1; c) S3 is the most photostable sensor in the currently studied core-shell fiber systems. The rate of photobleaching generally increases with increasing oxygen concentration due to the generation of reactive singlet oxygen, a dynamic quenching byproduct believed to be responsible for the photooxidation of probe molecules.[45] During the consumption of oxygen by adherent cells, the real photobleaching rate of the sensors applied in cell culture should fall somewhere between the 'Air' and 'No $O_2$' curves in Fig. 5. When oxygen-sensitive probes are dissolved in polymer matrix materials, the probe-probe and probe-host interactions not only determine the final sensing performance of the sensor but also the stability of the luminescence emission. It has been observed that when incorporated probe concentrations reach a critical value, the probes suffer from concentration quenching and triplet state annihilation.[46] This could explain the different photobleaching behaviors observed for S1 and S2. Although the probe concentration in S1 is lower than S2, poor solubility of the probe in PDMS matrix could cause local probe aggregation to accelerate photobleaching. S3 shows the best resistance to photobleaching among all three samples due both to the higher photostability of PtOEP [47] and – likely – excellent dispersion. It should be noted that for general applications of these sensors in cell culture, the total light exposure time needed to acquire oxygen concentrations will be far less than the duration of the tests in this study. In addition, these probes remain stable and active in the core-shell fibers during sensor fabrication, testing, storage and cell culture. The highly hydrophobic PDMS matrix and the protective PCL shell appear to prevent water penetration that might interfere with the performance of the probes. Cell viability and the lack of cytotoxicity also demonstrate the utility of incorporating probes inside these fibers.

**3.2.7. Biocompatibility—**As shown in Fig. 6, glioma cell morphology, association with the different types of fibers, and pattern of cell dispersion were essentially identical, with only slight visual differences. Since cell viability was not consistently affected (Fig. 7) we hypothesize that these small differences likely reflect differences in cell response to nanofiber modulus rather than effects of the nanofiber chemistry on the cells. Rao et al [48] have recently showed that the presence of a PDMS 'core' inside of a PCL 'shell' results in a higher modulus that can affect glioma cell adhesion and migration. This could explain the slightly more rounded morphology of glioma cells on PDMS-PCL and reduced cell adhesion

of the CNS1 line (Fig. 7). These differences, however, had no effect on migratory behavior, as indicated by the identical migration indexes of all cells analyzed on different fiber compositions. Cell viability, measured as the proportion of PI-positive to total cells showed an inconsistent pattern with one cell line unaffected (CNS1), another line showing reduced cell death in PDMS-PCL fibers (U251), and the third cell culture showing increased death (GBM 34). Again, these differences are likely a result of the differential response of the cells following adhesion to fibers of different modulus. It should be noted that cell death for established cell lines was consistently low (below 8% of total cells) while primary glioblastoma stem-like cells were considerably more affected, as expected. This strongly suggests a cell-specific response to the physical differences of the substrate rather than any consistent cytotoxicity due to the Pt porphyrin compound embedded in the fibers.

## 4. Conclusions

A new optical oxygen sensor is fabricated by the novel core-shell electrospinning of highly oxygen permeable polydimethylsiloxane within an envelope of biocompatible polycaprolactone. Fluorescent oxygen sensitive probes, tris(4,7-diphenyl-1,10-phenanthroline) ruthenium(II) and platinum octaethylporphyrin, are incorporated into this PDMS core. Fiber sensitivity can be adjusted depending on the chemistry, dispersion and inherent photon yield of the probes themselves. All sensors show rapid responses less than 0.5s due to the porous nature of electrospun fibers coupled with the relatively trivial diffusion barrier presented by the PDMS matrix. Linear calibration is achieved for both gaseous and dissolved oxygen over biologically relevant ranges. Sensing probes embedded in the fiber were shown to be stable throughout all tests and assessments. Glioma cell viability and migration experiments on these fibers show negligible biological effects of the sensing probes on the cells. These unique fiber-based sensors could be readily integrated to standard cell culture plates or bioreactors to provide critical oxygen information for both cancer cell research and engineered tissue growth.

## Acknowledgments

The project described was supported by Grant Number 1033991 from the National Science Foundation Chemical, Bioengineering, Environmental, and Transport Systems Division. The content is solely the responsibility of the authors and does not necessarily represent the official views of the National Science Foundation. R.X. and J.J.L are both full-time employees of The Ohio State University. P.B. and M.S.V. are employees of Brigham and Women's Hospital. The authors sincerely thank Professor Patricia Morris (Dept. of Materials Science and Engineering, The Ohio State University) for the use of her fluorescence microscope and Dr. E. Antonio Chiocca (Dept. of Neurosurgery, Brigham and Women's Hospital) for providing the original specimen and culture of GBM34 cells.

## Abbreviations

| | |
|---|---|
| **PDMS** | Polydimethylsiloxane |
| **PCL** | polycaprolactone |
| **Ru(dpp)(Cl)** | tris(4,7-diphenyl-1,10-phenanthroline) ruthenium(II) dichloride |
| **LED** | light emitting diode |
| **PtOEP** | platinum octaethylporphyrin |

| | |
|---|---|
| **RTV** | room-temperature vulcanizing |
| **Ru(dpp)(PB)** | tris(4,7-diphenyl-1,10-phenanthroline)ruthenium(II) tetraphenylboron |
| **HFP** | 1,1,1,3,3-hexafluoro-2-propanol |
| **DCM** | dichloromethane |
| **SEM** | scanning electron microscopy |

## References


1. Lopez-Barneo J, Pardal R, Ortega-Saenz P. Cellular mechanisms of oxygen sensing. Annu Rev Physiol. 2001; 63:259–287. [PubMed: 11181957]
2. Carmeliet P, Dor Y, Herbert J-M, Fukumura D, Brusselmans K, Dewerchin M, et al. Role of HIF-1[alpha]. in hypoxia-mediated apoptosis, cell proliferation and tumour angiogenesis. Nature. 1998; 394:485–490. [PubMed: 9697772]
3. Vaupel P, Schlenger K, Knoop C, Hockel M. OXYGENATION OF HUMAN TUMORS - EVALUATION OF TISSUE OXYGEN DISTRIBUTION IN BREAST CANCERS BY COMPUTERIZED O2 TENSION MEASUREMENTS. Cancer Res. 1991; 51:3316–3322. [PubMed: 2040005]
4. Brown JM, Wilson WR. Exploiting tumour hypoxia in cancer treatment. Nat Rev Cancer. 2004; 4:437–447. [PubMed: 15170446]
5. Gray LH, Conger AD, Ebert M, Hornsey S, Scott OCA. THE CONCENTRATION OF OXYGEN DISSOLVED IN TISSUES AT THE TIME OF IRRADIATION AS A FACTOR IN RADIOTHERAPY. Br J Radiol. 1953; 26:638–648. [PubMed: 13106296]
6. Pörtner, R.; Platas Barradas, OJ. Cultivation of Mammalian Cells in Fixed-Bed Reactors. In: Pörtner, R., editor. Animal Cell Biotechnology. Humana Press; 2007. p. 353-369.
7. Clark LC. MONITOR AND CONTROL OF BLOOD AND TISSUE OXYGEN TENSIONS. Transactions American Society for Artificial Internal Organs. 1956; 2:41-&.
8. Wang X, Chen H, Zhao Y, Chen X, Wang X. Optical oxygen sensors move towards colorimetric determination. TrAC, Trends Anal Chem. 2010; 29:319–338.
9. Amao Y. Probes and polymers for optical sensing of oxygen. Microchim Acta. 2003; 143:1–12.
10. Florescu M, Katerkamp A. Optimisation of a polymer membrane used in optical oxygen sensing. Sensors and Actuators B: Chemical. 2004; 97:39–44.
11. Grist SM, Chrostowski L, Cheung KC. Optical Oxygen Sensors for Applications in Microfluidic Cell Culture. Sensors. 2010; 10:9286–9316. [PubMed: 22163408]
12. Alford PC, Cook MJ, Lewis AP, McAuliffe GSG, Skarda V, Thomson AJ, et al. Luminescent metal complexes. Part 5. Luminescence properties of ring-substituted 1,10-phenanthroline tris-complexes of ruthenium(II). Journal of the Chemical Society, Perkin Transactions. 1985; 20:705–709.
13. Bacon JR, Demas JN. DETERMINATION OF OXYGEN CONCENTRATIONS BY LUMINESCENCE QUENCHING OF A POLYMER-IMMOBILIZED TRANSITION-METAL COMPLEX. Anal Chem. 1987; 59:2780–2785.
14. Koren K, Borisov SM, Saf R, Klimant I. Strongly Phosphorescent Iridium(III)–Porphyrins – New Oxygen Indicators with Tuneable Photophysical Properties and Functionalities. Eur J Inorg Chem. 2011; 2011:1531–1534. [PubMed: 22485072]
15. Kalyanasundaram K. Photochemistry of Polypyridine and Porphyrin: Academic Press. 1992
16. Chu C, Lo Y. Highly sensitive and linear calibration optical fiber oxygen sensor based on Pt(II) complex embedded in sol-gel matrix. Sensors and Actuators B-Chemical. 2011; 155:53–57.
17. He H, Fraatz RJ, Leiner MJP, Rehn MM, Tusa JK. Selection of silicone polymer matrix for optical gas sensing. Sensors and Actuators B: Chemical. 1995; 29:246–250.

18. Hartmann P, Leiner MJP, Lippitsch ME. LUMINESCENCE QUENCHING BEHAVIOR OF AN OXYGEN SENSOR-BASED ON A RU(II) COMPLEX DISSOLVED IN POLYSTYRENE. Anal Chem. 1995; 67:88–93.
19. Hartmann P, Trettnak W. Effects of polymer matrices on calibration functions of luminescent oxygen sensors based on porphyrin ketone complexes. Anal Chem. 1996; 68:2615–2620. [PubMed: 21619209]
20. Tian YQ, Shumway BR, Gao WM, Youngbull C, Holl MR, Johnson RH, et al. Influence of matrices on oxygen sensing of three sensing films with chemically conjugated platinum porphyrin probes and preliminary application for monitoring of oxygen consumption of Escherichia coli (E coli). Sensors and Actuators B-Chemical. 2010; 150:579–587.
21. DeGraff, BA.; Demas, JN. Luminescence-Based Oxygen Sensors Reviews in Fluorescence 2005. Geddes, CD.; Lakowicz, JR., editors. Springer US: 2005. p. 125-151.
22. Ratner, RD.; Hoffman, AS.; Schoen, FJ.; Lemons, JE. Biomaterials science: an introduction to materials in medicine. Second ed.. Elsevier Academic Press; 2004.
23. Agudelo-Garcia PA, De Jesus JK, Williams SP, Nowicki MO, Chiocca EA, Liyanarachchi S, et al. Glioma Cell Migration on Three-dimensional Nanofiber Scaffolds Is Regulated by Substrate Topography and Abolished by Inhibition of STAT3 Signaling. Neoplasia. 2011; 13:831–U96. [PubMed: 21969816]
24. Kim YB, Cho D, Park WH. Electrospinning of poly(dimethyl siloxane) by sol–gel method. J Appl Polym Sci. 2009; 114:3870–3874.
25. Lannutti J, Reneker D, Ma T, Tomasko D, Farson D. Electrospinning for tissue engineering scaffolds. Materials Science and Engineering C. 2007; 27:504–509.
26. Mills A, Thomas M. Fluorescence-based thin plastic film ion-pair sensors for oxygen. Analyst. 1997; 122:63–68.
27. Klimant I, Wolfbeis OS. OXYGEN-SENSITIVE LUMINESCENT MATERIALS BASED ON SILICONE-SOLUBLE RUTHENIUM DIIMINE COMPLEXES. Anal Chem. 1995; 67:3160–3166.
28. Wu WH, Ji SM, Wu WT, Guo HM, Wang X, Zhao JZ, et al. Enhanced luminescence oxygen sensing property of Ru(II) bispyridine complexes by ligand modification. Sensors and Actuators B-Chemical. 2010; 149:395–406.
29. Demas JN, DeGraff BA. Design and applications of highly luminescent transition metal complexes. Anal Chem. 1991; 63:829A–837A.
30. Zhang H, Lei B, Mai W, Liu Y. Oxygen-sensing materials based on ruthenium(II) complex covalently assembled mesoporous MSU-3 silica. Sensors and Actuators B-Chemical. 2011; 160:677–683.
31. Klimant I, Kuhl M, Glud RN, Holst G. Optical measurement of oxygen and temperature in microscale: strategies and biological applications. Sensors and Actuators B-Chemical. 1997; 38:29–37.
32. Lee SK, Okura I. Photoluminescent determination of oxygen using metalloporphyrin-polymer sensing systems. Spectrochimica Acta Part a-Molecular and Biomolecular Spectroscopy. 1998; 54:91–100.
33. Rongsheng C, Farmery AD, Obeid A, Hahn CEW. A Cylindrical-Core Fiber-Optic Oxygen Sensor Based on Fluorescence Quenching of a Platinum Complex Immobilized in a Polymer Matrix. Sensors Journal, IEEE. 2012; 12:71–75.
34. Yeh TS, Chu CS, Lo YL. Highly sensitive optical fiber oxygen sensor using Pt(II) complex embedded in sol-gel matrices. Sensors and Actuators B-Chemical. 2006; 119:701–707.
35. Thomas PC, Halter M, Tona A, Raghavan SR, Plant AL, Forry SP. A Noninvasive Thin Film Sensor for Monitoring Oxygen Tension during in Vitro Cell Culture. Anal Chem. 2009; 81:9239–9246. [PubMed: 19860390]
36. Gillanders RN, Tedford MC, Crilly PJ, Bailey RT. Thin film dissolved oxygen sensor based on platinum octaethylporphyrin encapsulated in an elastic fluorinated polymer. Analytica Chimica Acta. 2004; 502:1–6.

37. Carraway ER, Demas JN, Degraff BA, Bacon JR. PHOTOPHYSICS AND PHOTOCHEMISTRY OF OXYGEN SENSORS BASED ON LUMINESCENT TRANSITION-METAL COMPLEXES. Anal Chem. 1991; 63:337–342.

38. Bedlek-Anslow JM, Hubner JP, Carroll BF, Schanze KS. Micro-heterogeneous Oxygen Response in Luminescence Sensor Films. Langmuir. 2000; 16:9137–9141.

39. Reneker, DH.; Yarin, AL.; Zussman, E.; Xu, H. Electrospinning of Nanofibers from Polymer Solutions and Melts. In: Hassan, A.; Erik van der, G., editors. Advances in Applied Mechanics. Elsevier; 2007. p. 43-346.

40. Wang Y, Li B, Zhang L, Zuo Q, Li P, Zhang J, et al. High-Performance Oxygen Sensors Based on Eu-III Complex/Polystyrene Composite Nanofibrous Membranes Prepared by Electrospinning. ChemPhysChem. 2011; 12:349–355. [PubMed: 21275027]

41. Wang Y, Li B, Liu Y, Zhang L, Zuo Q, Shi L, et al. Highly sensitive oxygen sensors based on Cu(I) complex-polystyrene composite nanofibrous membranes prepared by electrospinning. Chemical Communications. 2009:5868–5870. [PubMed: 19787124]

42. Wang L-Y, Xu Y, Lin Z, Zhao N, Xu Y. Electrospinning fabrication and oxygen sensing properties of Cu(I) complex-polystyrene composite microfibrous membranes. Journal of Luminescence. 2011; 131:1277–1282.

43. Acosta MA, Ymele-Leki P, Kostov YV, Leach JB. Fluorescent microparticles for sensing cell microenvironment oxygen levels within 3D scaffolds. Biomaterials. 2009; 30:3068–3074. [PubMed: 19285719]

44. Wang XD, Gorris HH, Stolwijk JA, Meier RJ, Groegel DBM, Wegener J, et al. Self-referenced RGB colour imaging of intracellular oxygen. Chemical Science. 2011; 2:901–906.

45. Hartmann P, Leiner MJP, Kohlbacher P. Photobleaching of a ruthenium complex in polymers used for oxygen optodes and its inhibition by singlet oxygen quenchers. Sensors and Actuators B: Chemical. 1998; 51:196–202.

46. Milosavljevic BH, Thomas JK. Photochemistry of compounds adsorbed into cellulose. 1. Decay of excited tris(2,2'-bipyridine)ruthenium(II). The Journal of Physical Chemistry. 1983; 87:616–621.

47. Shinar R, Zhou Z, Choudhury B, Shinar J. Structurally integrated organic light emitting device-based sensors for gas phase and dissolved oxygen. Analytica Chimica Acta. 2006; 568:190–199. [PubMed: 17761260]

48. Rao SS, Nelson MT, Xue R, DeJesus JK, Viapiano MS, Lannutti JJ, et al. Mimicking white matter tract topography using core–shell electrospun nanofibers to examine migration of malignant brain tumors. Biomaterials. 2013; 34:5181–5190. [PubMed: 23601662]

## Biographies

Ruipeng Xue received his BE degree from University of Science and Technology Beijing, China in 2007 and his MS degree from Stony Brook University, USA in 2010. He is currently a PhD candidate in Materials Science and Engineering at The Ohio State University. His research focuses on the development of nanofiber-based multifunctional materials for biosensing and structural applications.

Prajna Behera completed her BS in Zoology in 2005 and MS in Biotechnology in 2007 from India. She was a Senior Research Fellow at the Institute of Post-Graduate Medical Education and Research (IPGMER) in Kolkata from 2008 to 2011, investigating mechanisms of neurodegeneration and co-authoring several peer-reviewed publications. She joined the Viapiano laboratory as a Senior Research Associate in 2012 focused on studying mechanisms of glioma cell motility and developing and testing novel technologies assessing cell migration/invasion.

Joshua Xu was at the time of this work a high-achieving student at Dublin Jerome High School having interests in the interaction of medicine and materials as a means of addressing biomedical problems. After graduating summa cum laude he has since been admitted to Northwestern University and the McCormick School of Engineering and Applied Science.

Mariano Viapiano received a BS degree in Molecular Biology from the University of Buenos Aires (Argentina) in 1993 and completed his PhD in Neuroscience there in 1998. He trained as a postdoctoral fellow at the University of Sao Paulo and Yale University. He then became an assistant Professor of Neurosurgery at The Ohio State University from 2006 until 2012. In October 2012 he became Assistant Professor of Neurosurgery and Research Director of the Harvey Cushing Neuro-Oncology Laboratories at the Brigham and Women's Hospital and Harvard Medical School. He has more than a decade of experience in glioma biology with particular emphasis on the mechanisms of tumor cell invasion and physical interaction with the microenvironment. He has published over 30 refereed articles and reviews.

John Lannutti received MS and BS degrees from the University of Florida in 1982 and 1984, respectively, and his PhD from the University of Washington (Seattle) in 1990. He then joined the faculty of the Materials Science and Engineering department at Ohio State in 1990. He has more than 25 years of experience in materials processing involving both Silicon Valley and academia. Dr. Lannutti's career has recently utilized 10+ years of experience in electrospinning for biological applications to focus in on the fabrication and synthesis of advanced biosensing nanofiber materials for applications in cancer research and prevention. He holds six patents and has published more than 150 refereed journal papers.

## Highlights

- PDMS ‘core’ nanofibers can be created via encapsulation within a PCL ‘shell.’
- PDMS is ideal for oxygen sensing as it allows for very rapid oxygen diffusion.
- These nanofibers display a perfectly linear response to oxygen.
- The rate of response to oxygen is 4–10 times faster than previous reports.
- Pt-based porphyrin in a PDMS core does not cause significant cytotoxicity nor affect cell behavior

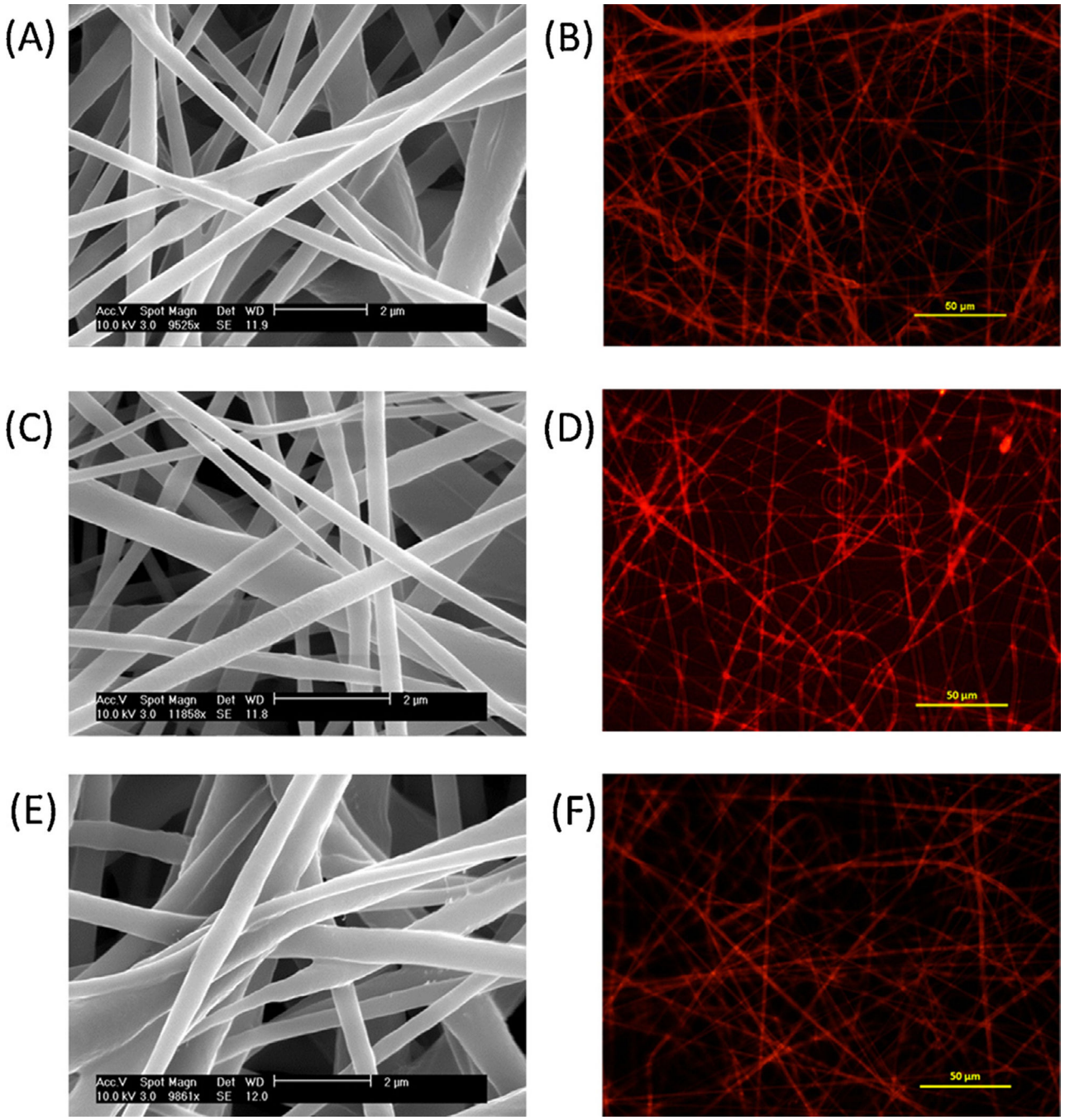


**Fig. 1.**
SEM and fluorescent images of PDMS-PCL fibers: (A) (B) S1, (C) (D) S2 and (E) (F) S3.

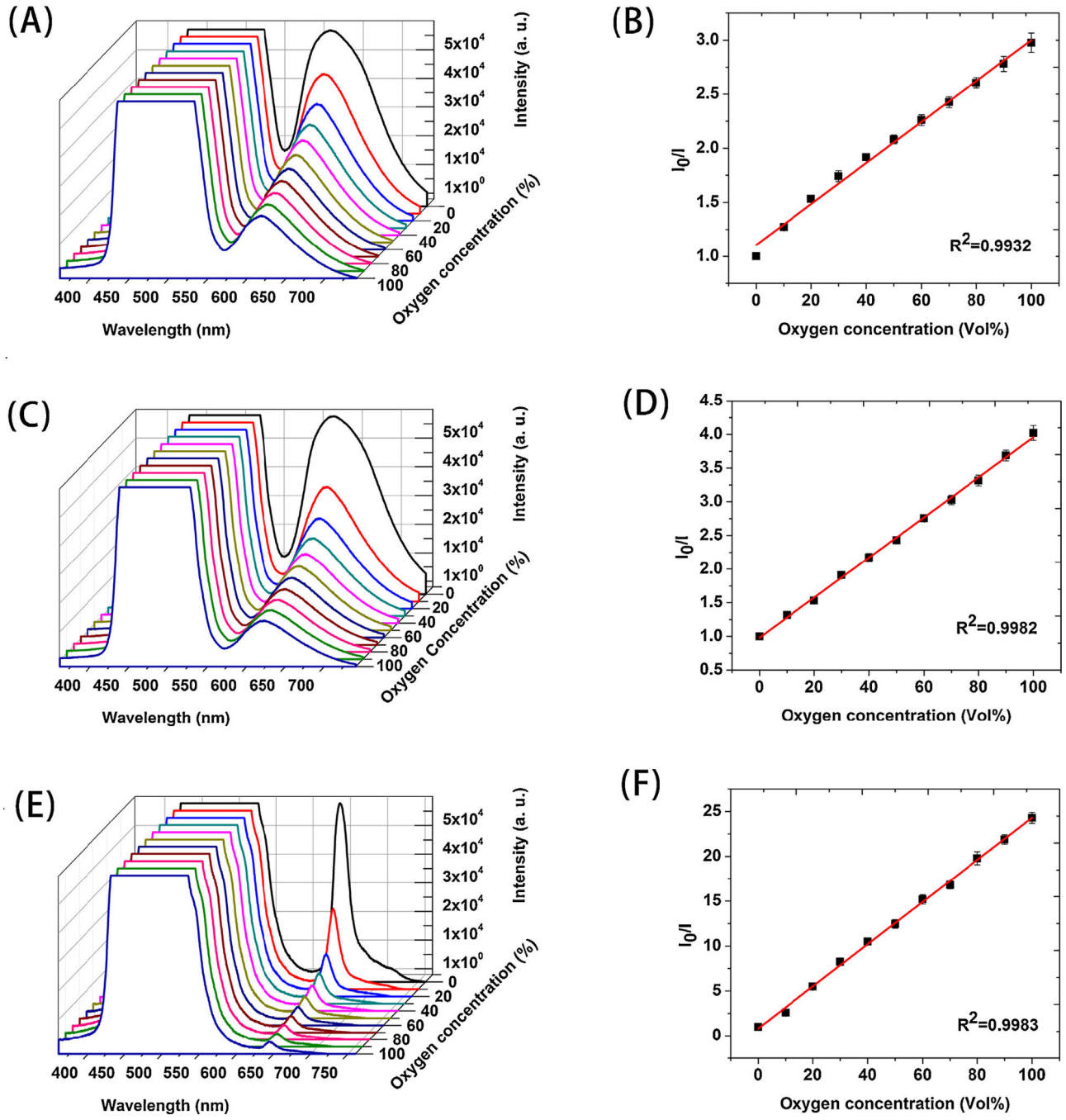


**Fig. 2.**

oxygen and corresponding Stern-Volmer plot for PDMS-PCL fibers: (A) (B) S1, (C) (D) S2 and (E) (F) S3.

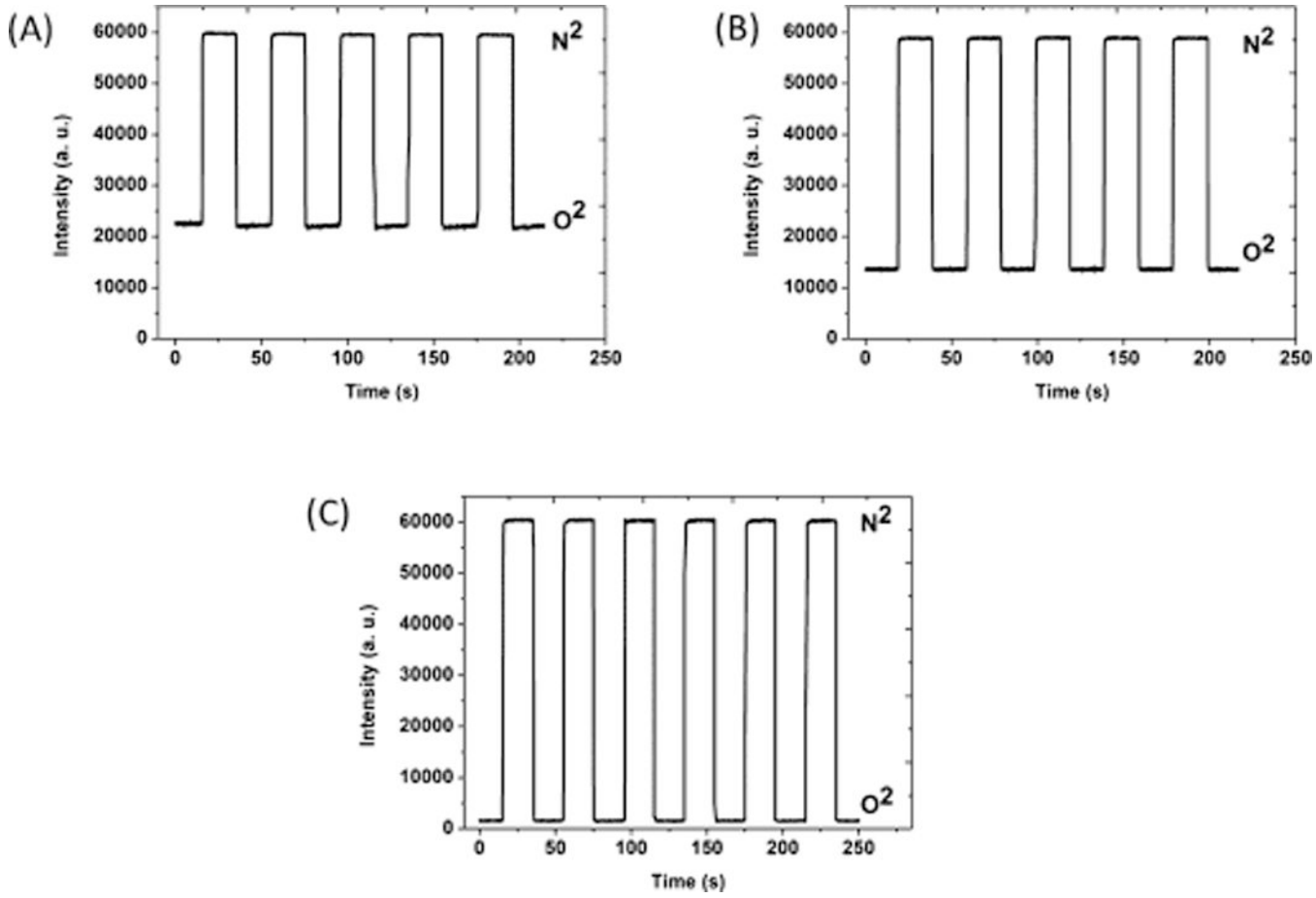


**Fig. 3.**

Reversibility of PDMS-PCL sensors (A) S1, (B) S2 and (C) S3 to alternating nitrogen and oxygen gas.

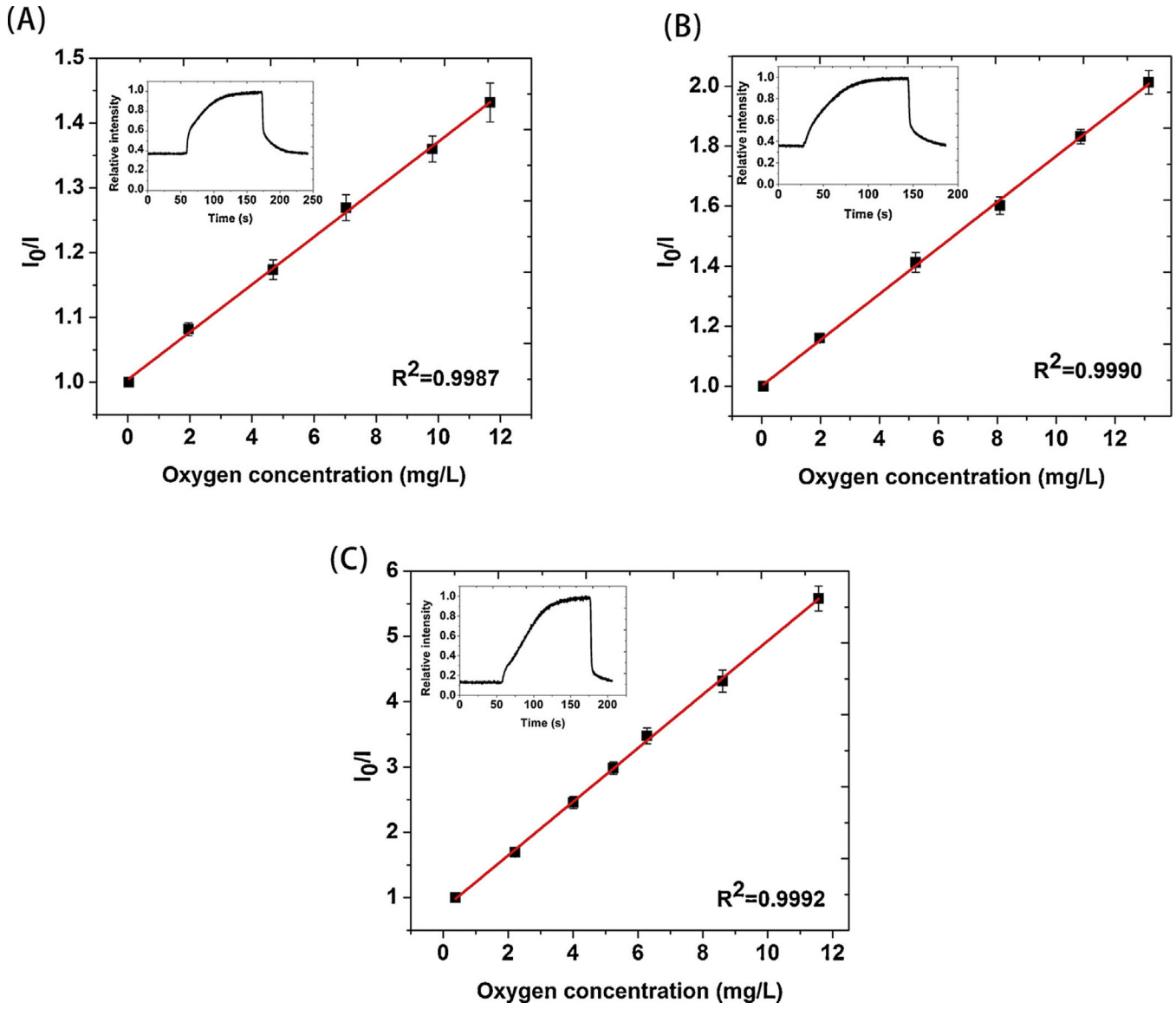


**Fig. 4.**

Stern-Volmer plot of PDMS-PCL sensor response (including error bars) to dissolved oxygen (A) S1, (B) S2 and (C) S3. The Figure inserts report their continuous responses when the water was consecutively saturated by oxygen/nitrogen/oxygen etc.

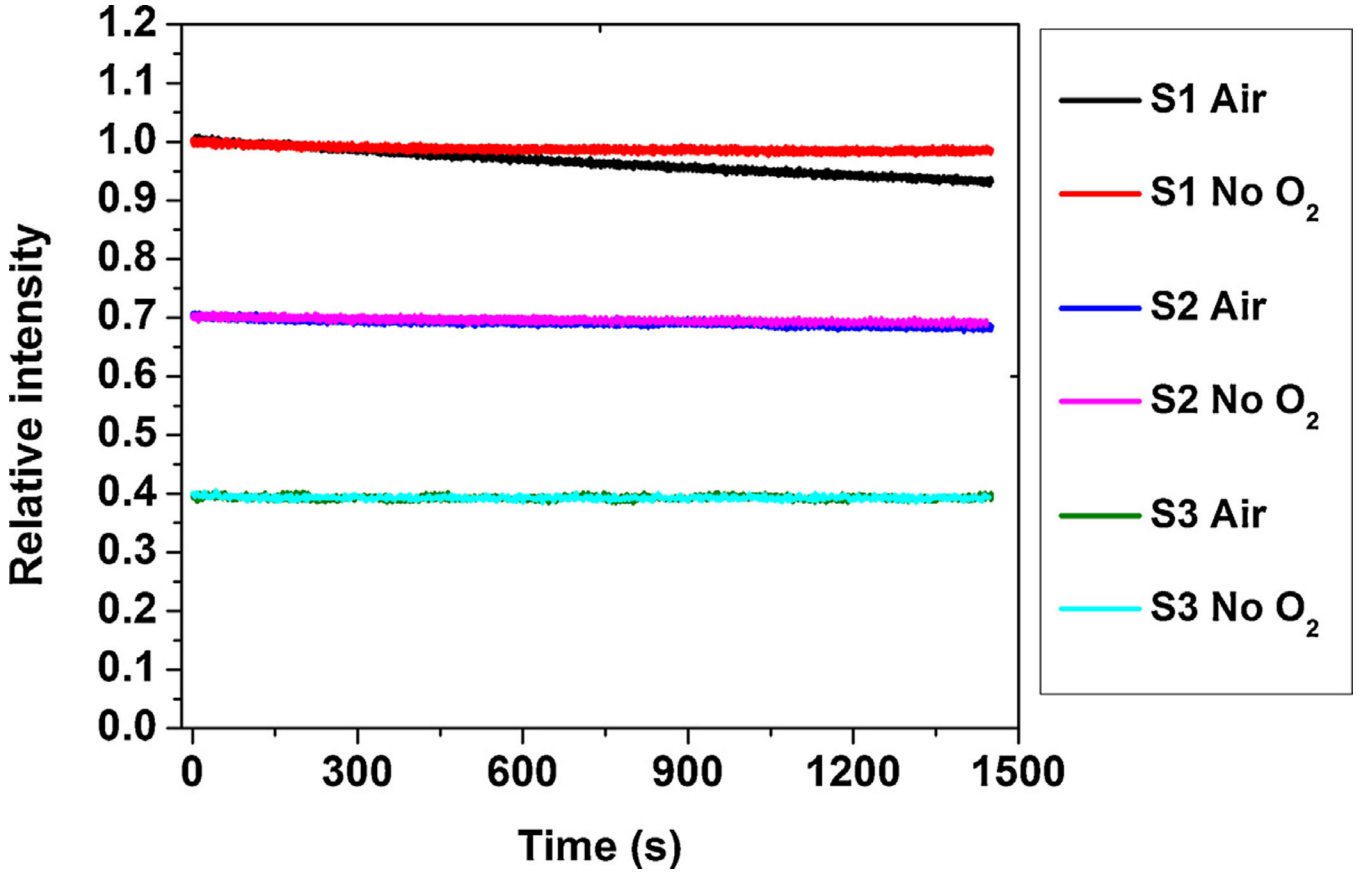


**Fig. 5.**
Photostability tests for PDMS-PCL core-shell fibers in air saturated and oxygen-free water.

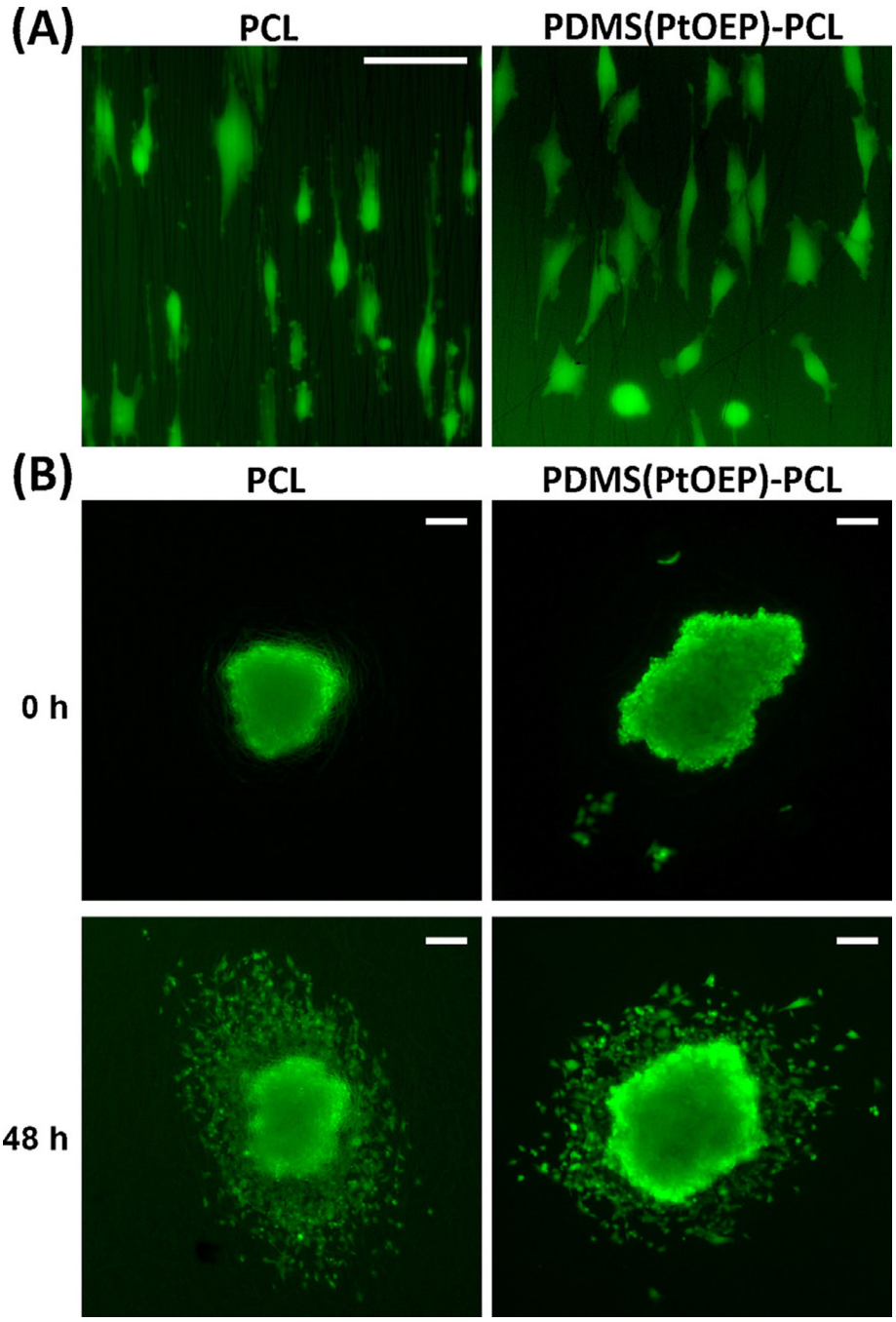


**Fig. 6.**

Cell morphology and dispersion on PCL nanofibers versus PDMS(PtOEP)-PCL nanofibers. (A) U251 cells show similar morphology and stretching over PCL and PDMS(PtOEP)-PCL fibers (bar: 50 μm). (B) Tumorspheres of U251 cells imaged immediately after deposition on randomly-aligned nanofibers and 48 hours later. Note the radial pattern of cell dispersion, which is similar in both types of fibers (bars: 100 μm).

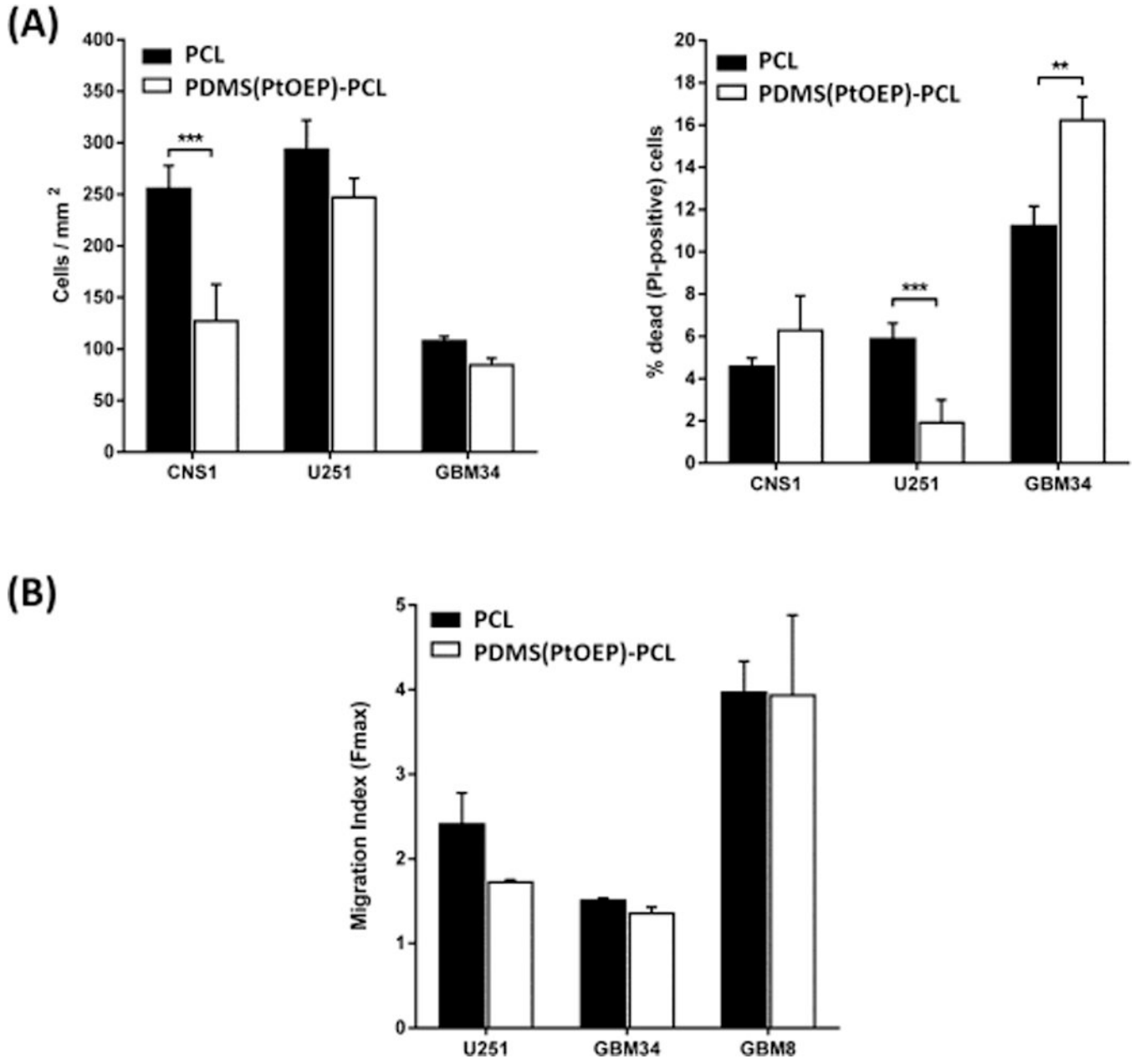


**Fig. 7.**

Cell viability and migration are quantitatively similar in PCL and PDMS(PtOEP)-PCL nanofibers. (A) Analysis of cell viability (number of calcein-positive cells/mm$^2$) and cell death (% of PI-positive cells/total cells per well) reveal few significant changes, none of which show a consistent trend. (B) Analysis of cell migration (dispersion at 48h compared to the radius of original tumorsphere) indicates that the migratory behavior is not affected by the presence of the Pt porphyrin probe.

**Table 1**

Specifications of PDMS–PCL core-shell fibers.

| Sample | Probe | PDMS | Ratio | Diameter (nm) | Emission peak (nm) |
|---|---|---|---|---|---|
| S1 | Ru(dpp)(Cl) | two-part | 1:1000 | 512 ± 195 | 618 |
| S2 | Ru(dpp) (PB) | moisture cure | 1:200 | 401 ± 131 | 622 |
| S3 | PtOEP | moisture cure | 1:200 | 570 ± 192 | 645 |